OPEN ACCESS
JOURNAL OF ADVANCED DIELECTRICS
Vol. 14, No. 1 (2024) 2245001 (9 pages)

DOI: 10.1142/S2010135X22450011

Energy storage optimization of ferroelectric ceramics during phase-transition process of amorphous/nanocrystalline and polycrystalline by using a phase-field model for dielectric breakdown

Suilong Huang[*,†], Jianwen Chen[*,‖], Zhen Su[‡], Xiucai Wang[§], Wenbo Zhu[†], Wenjun Chen[*], Xinmei Yu[*] and Peng Xiao[¶]

[*]*School of Electronic and Information Engineering, Foshan University*
Foshan 528000, P. R. China

[†]*School of Mechatronic Engineering and Automation, Foshan University*
Foshan 528000, P. R. China

[‡]*China-Australia Institute for Advanced Materials and Manufacturing, Jiaxing University*
Jiaxing 314001, P. R. China

[§]*School of Materials Science and Hydrogen Energy, Foshan University*
Foshan 528000, P. R. China

[¶]*School of Physics and Optoelectronic Engineering, Foshan University*
Foshan 528000, P. R. China

[‖]iamjwen@126.com

Received 22 July 2022; Revised 10 September 2022; Accepted 13 September 2022; Published 21 October 2022

Ferroelectric ceramics have the potential to be widely applied in the modern industry and military power systems due to their ultrafast charging/discharging speed and high energy density. Considering the structural design and electrical properties of ferroelectric capacitor, it is still a challenge to find out the optimal energy storage of ferroelectric ceramics during the phase-transition process of amorphous/nanocrystalline and polycrystalline. In this work, a finite element model suitable for the multiphase ceramic system is constructed based on the phase field breakdown theory. The nonlinear coupling relationship of multiple physical fields between multiphase ceramics was taken into account in this model. The basic structures of multiphase ceramics are generated by using the Voronoi diagram construction method. The specified structure of multiphase ceramics in the phase- transition process of amorphous/nanocrystalline and polycrystalline was further obtained through the grain boundary diffusion equation. The simulation results show that the multiphase ceramics have an optimal energy storage in the process of amorphous polycrystalline transformation, and the energy storage density reaches the maximum when the crystallinity is 13.96% and the volume fraction of grain is 2.08%. It provides a research plan and idea for revealing the correlation between microstructure and breakdown characteristics of multiphase ceramics. This simulation model realizes the nonlinear coupling of the multiphase ceramic mesoscopic structure and the phase field breakdown. It provides a reference scheme for the structural design and performance optimization of ferroelectric ceramics.

Keywords: Ferroelectric ceramics; phase transition; phase-field model; dielectric breakdown; energy storage.

1. Introduction

In recent years, with the development of the energy industry and electronic power technology, high-performance dielectric capacitors with ultrafast charging/discharging speed and high energy density dielectric capacitors are desired.[1–9] However, the dielectric capacitors still suffer from a low energy density.[10–12] Generally, the energy storage density (W) of a dielectric capacitor is determined by the applied electric field (E) and the induced electric displacement (D), which is described by the expression as $W = \int EdD$.[13–15] Obviously, permittivity and dielectric strength play an important role in energy storage. Ferroelectric materials with high permittivity have been extensively studied, and a large number of related materials have been developed and processed.[16–20] However, many factors are weakening the breakdown behavior under the Cask Effect Theory, which involves engineering problems of a multiscale system such as nanoscopic, microscopic, mesoscopic and macroscopic.[21–24] Current studies have found that the breakdown field strength of most inorganic ferroelectric films is lower than 3000 kV $\cdot$ cm^{-1}.[25–28] Specifically, the breakdown field strength of current commercial ferroelectric ceramics is much lower than its intrinsic breakdown strength,

‖Corresponding author.

and the average dielectric strength of ferroelectric thin films is only 2600 kV · cm^{-1}.[29–32] How to improve the dielectric strength of ferroelectric ceramics is the core issue to optimize its energy storage density.

Ferroelectric ceramics undergo phase transition during heat treatment, and the change of microstructures can influence the breakdown characteristics.[33,34] Therefore, based on the breakdown theory and the simulation, it is significant to systematically explore the correlative mechanism between phase transition and breakdown characteristics for optimizing the energy storage density of ferroelectric ceramics. The dielectric breakdown models include intrinsic breakdown, avalanche breakdown, thermal breakdown, electromechanical breakdown, electrochemical breakdown and erosion breakdown.[35,36] The theoretical basis of intrinsic breakdown and avalanche breakdown is the electron impact ionization criterion. Thermal breakdown is caused by the accumulation of molecular polarization heat, which causes the heating speed to be larger than the heat dissipation speed ratio, thereby triggering it.[37,38]

For the study of ferroelectric energy storage materials and devices, the phase-field model oriented to the mesoscopic scale is the most concise and effective theoretical calculation method. At present, the phase-field model for dielectric breakdown is mainly constructed based on the electrostatic breakdown theory with energy as the criterion, and the electrical treeing, breakdown strength, and energy storage density are calculated by simulating the breakdown process.[39–41] Clarifying the relationship between the phase transition of the ferroelectric ceramics and the energy storage density is significant to obtain the microstructure for the optimal energy storage characteristics.

In this work, a method was proposed to simulate the process of phase transition. The method couple phase-field for dielectric breakdown model with the microstructures during the phase transition to explore the correlative mechanism of microstructure on energy storage characteristics. Through the simulation model, the effects of different microstructures on the breakdown characteristics during the process of phase transition were investigated.

2. The Model

This paper builds a phase-field model referring to Pitike and Hong.[42,43] The phase-field model of electrical damage initiation and propagation in dielectric solids is established using the analogy of dielectric breakdown and solid fracture with the coupling relationship of multiple physical fields in multiphase ceramics.[44,45] Cai explored the effect of microstructure on breakdown behavior from the perspective of grain size.[46] Compared with the work, this paper simulates the microstructural changes of phase transition more systematically. Herein, a method combining Voronoi diagram and boundary diffusion equation is used to simulate the microstructure of ferroelectric ceramics during phase transition. The basic structures of multiphase ceramics are generated by using Voronoi diagram construction method. The specify structure of multiphase ceramics in phase transition process of amorphous/nanocrystalline and polycrystalline was further obtained through the grain boundary diffusion equation. Various microstructures are simulated systematically during phase transition of ferroelectric ceramics by the models.

In the phase-field model for dielectric breakdown, we introduce the scalar s to express the degree of damage in the evolution process. The value of s ranges from 0 to 1, which corresponds to the complete damage state to the intact state of the phase field. The completely damaged part will become high-dielectric permittivity. During the evolution process, the dielectric permittivity can be expressed as follows:

$$\varepsilon(s) = \frac{\varepsilon_{\text{ini}}}{f(s) + \eta}, \tag{1}$$

where $f(s) = 4s^3 - 3s^4$. ε_{ini} is the initial dielectric permittivity. To make $\varepsilon(s)$ a maximum value when $f(s) = 0$, η is taken as a small enough number (10^{-3}). In this paper, the main research object is ferroelectric ceramics, which contain crystal grains and grain boundaries. The relationship between the relative permittivity of the crystal grain and the electric field can be expressed as follows:[47]

$$\varepsilon_g(E) = \frac{\varepsilon_g(0)}{\left(1 + kE^2\right)^{\frac{1}{3}}}, \tag{2}$$

where $\varepsilon_g(0)$ is the relative permittivity of the zero-field, which is set to 10. The parameter k is the material constant, here, it is taken as $k = 3\beta\varepsilon_{gb}^3$. β is the John's constant, which is 1, and ε_{gb} is the relative permittivity of the grain boundary, which is 1. Therefore, the permittivity of the phase-field model of ferroelectric ceramics can be expressed as follows:

$$\varepsilon_{\text{ini}}(E) = \begin{cases} \dfrac{\varepsilon_{g(0)}}{\left(1 + kE^2\right)^{\frac{1}{3}}} & \text{in grain,} \\ \varepsilon_{gb} & \text{on grain boundary.} \end{cases} \tag{3}$$

In the evolution of the breakdown process, the total potential energy of the system can be expressed as follows:

$$\Pi[s, x_i] = \int_{\Omega} \left[W_{\text{es}}(E, s) + W_d(s) + W_i\left(\frac{\partial s}{\partial x_i}\right) \right] dV. \tag{4}$$

In the total potential energy expression (4), W_{es} is the complementary electrostatic potential energy per unit volume,

$$W_{\text{es}}(E, s) = \begin{cases} -\displaystyle\int_0^{E_{\max}} \frac{\varepsilon_0 \varepsilon_g(s) E}{\left(1 + kE^2\right)^{\frac{1}{3}}} dE & \text{in grain,} \\ -\dfrac{\varepsilon_0 \varepsilon_{gb}(s)}{2} E \cdot E & \text{on grain boundary.} \end{cases} \tag{5}$$

The damage energy is $W_d(s) = W_c\,[1 - f(s)]$, where W_c is the critical density of electrostatic energy. W_i is a gradient energy term used to adjust the sharp phase boundaries. The gradient energy term can be expressed as follows:

$$W_i\left(\frac{\partial s}{\partial x_i}\right) = \frac{\Gamma}{4}\frac{\partial s}{\partial x_i}\cdot\frac{\partial s}{\partial x_i}, \tag{6}$$

where Γ can be approximated as breakdown energy.

By assuming the linear dynamic equation: $\frac{\partial s}{\partial t} = -m\frac{\delta \Pi}{\delta s}$, we can get the normalized dimensionless governing equation (7) for linear dielectric and equation (8) for nonlinear dielectric in breakdown propagation:

$$\begin{cases} \dfrac{\partial}{\partial \bar{x}_i}\left[\dfrac{1}{f(s)+\eta}\dfrac{\partial \bar{\phi}}{\partial \bar{x}_i}\right] = 0, \\ \dfrac{\partial s}{\partial \bar{t}} = -\dfrac{f'(s)}{2\left[f(s)+\eta\right]^2}\dfrac{\partial \bar{\phi}}{\partial \bar{x}_i}\dfrac{\partial \bar{\phi}}{\partial \bar{x}_i} + f'(s) + \dfrac{1}{2}\dfrac{\partial^2 s}{\partial \bar{x}_i \partial \bar{x}_i}, \end{cases} \tag{7}$$

$$\begin{cases} \dfrac{\partial}{\partial \bar{x}_i}\left[\varepsilon_g(s)\left(1+\dfrac{\partial \bar{\phi}}{\partial \bar{x}_i}\dfrac{\partial \bar{\phi}}{\partial \bar{x}_i}\bar{k}\right)^{-\frac{1}{3}}\dfrac{\partial \bar{\phi}}{\partial \bar{x}_i}\right] = 0, \\ \dfrac{\partial s}{\partial \bar{t}} = -\dfrac{3\varepsilon_g'(s)}{4\bar{k}}\left(\left(1+\dfrac{\partial \bar{\phi}}{\partial \bar{x}_i}\dfrac{\partial \bar{\phi}}{\partial \bar{x}_i}\bar{k}\right)^{\frac{2}{3}} - 1\right) + f'(s) + \dfrac{1}{2}\dfrac{\partial^2 s}{\partial \bar{x}_i \partial \bar{x}_i}. \end{cases} \tag{8}$$

The $\bar{k}$ of these equations is a nonlinear factor, and the line marked with a horizontal line is the dimensionless counterpart of the corresponding quantity. Through Eqs. (7) and (8), the propagation process of the electrical treeing can be calculated in COMSOL Multiphysics 5.5.

In this work, to systematically discuss the effect of microstructure on breakdown characteristics, the phase transition process of ferroelectric ceramics is mainly divided into two stages to study. The first stage is mainly reflected in the change of crystallinity. The second stage is mainly reflected in the change of grain size. As shown in Fig. 1, the phase transition process is divided into multiple states from S0 to S5 and N1 to N6. S0 refers to the models with dielectric of pure phase. Samples from S0 to S5 represent the phase-field models with gradually increasing crystallinity, respectively. The microstructures of N1–N6 with growing grain size are shown in Fig. 1. Herein, the crystallinity is calculated as the ratio of the crystallization area to the total area. The simulation result in N1–N6 is discussed with average gain size. Finally, the average gain size will be converted to volume fraction of grain to express. Combining the above microstructure and the phase-field model for dielectric breakdown, this work structures several models for dielectric breakdown and simulate the breakdown characteristic changes in the phase transition process of ferroelectric ceramic.

3. Results and Discussions

In this section, the dielectric breakdown process with different microstructures during phase transition will be studied and various characteristics of ferroelectric ceramics in the simulation for dielectric breakdown will be discussed to obtain the microstructure of optimal energy storage. Examples in this section are calculated by implementing Eqs. (6)–(8) into the commercial finite element software COMSOL 5.5. The potential field is interpolated by quadratic Lagrange elements and the damage field is interpolated by linear Lagrange elements to achieve compatibility. All samples are calculated in a two-dimensional rectangular domain with a width of 40 and a height of 60.

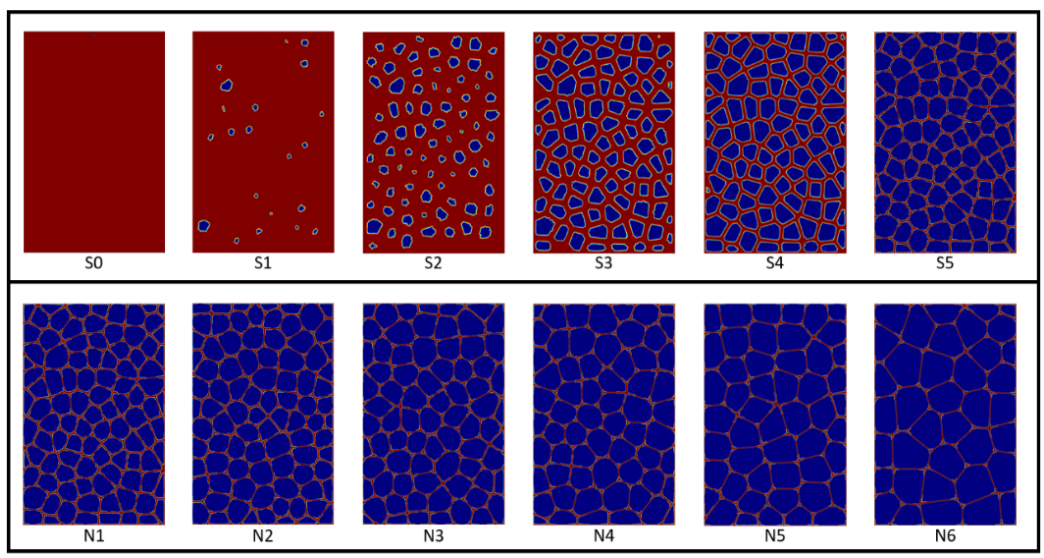

Fig. 1. (S0–S5) The two-dimensional microstructure of phase-field model in the first stage of transition process (N1–N6) the two-dimensional microstructure of phase-field model in the second stage of transition process.

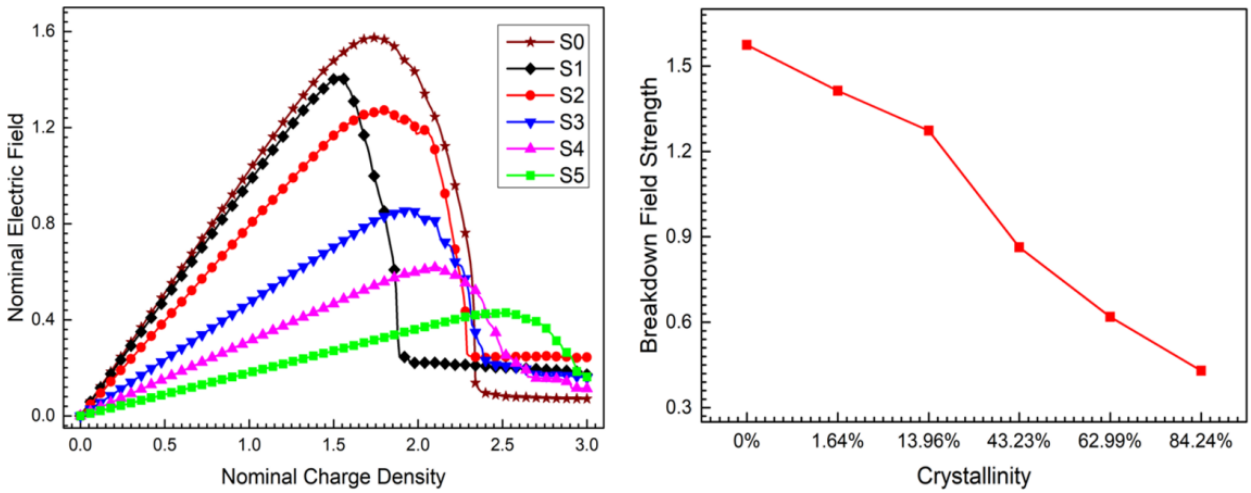

(a) (b)

Fig. 2.(a) Field-charge-density relation with S0–S5. (b) The relationship between crystallinity and breakdown field strength with S0–S5.

3.1. *The First Stage from S0 to S5*

In Fig. 2(a), the change of the nominal electric field during the breakdown process of the phase-field models with S0–S5 is shown and the ordinate is the average electric field strength of the surface. Figure 2(b) shows the change of the crystallinity and breakdown field strength with the corresponding phase-field model. As shown in Fig. 2(a), before reaching the breakdown condition, the electric field increases linearly with the increase of charge and the dielectric characteristics are relatively stable. The damage field begins to appear after reaching the breakdown condition and the electric field begins to decline rapidly. The strength of the electric field reaches the breakdown condition as the breakdown field strength. With the increasing crystallinity from S0 to S5, the change rate of average field intensity before reaching the breakdown field strength also decreases. The dielectric breakdown behavior of samples occurs with increasing charge density. The specific corresponding parameters are shown in Table 1. The model started to breakdown roughly at Q1. As shown in Fig. 2(b), the breakdown field strength decreases with the increase of crystallinity. Namely, the higher the crystallinity of the phase transition process, the smaller the breakdown field strength that can be achieved by the phase-field model, while more charges are required for breakdown.

The evolution of phase-field for dielectric breakdown is shown in Fig. 3. The column direction in Fig. 3 is the evolution of dielectric breakdown with increased charge density, respectively. The row direction in Fig. 3 is six phase-field models for dielectric breakdown with S0–S5. The nominal charge densities from Q0 to Q3 at the corresponding moments are shown as Table 1. The curves with different colors are equipotential lines which represent the electric field. The legend of the right side shows the colors distribution of equipotential lines in different electric field intensities.

From a vertical perspective in the S0 and S1, the electrical treeing appears from the high potential to low potential. The potential at the tip of the electrical treeing is high. In the S2, the electrical treeing is evolved with branches. In the models from S3 to S5, the electrical treeing appears in multiple

Table 1. The corresponding nominal charge density in evolution process with S0–S5.

Charge density	S0	S1	S2	S3	S4	S5
Q1	0.23	0.32	0.34	0.38	0.40	0.48
Q2	1.74	1.5	1.9	2.0	2.3	2.65
Q3	2.21	1.8	2.35	2.4	2.5	2.9
Q4	3.0	3.0	3.0	3.0	3.0	3.0

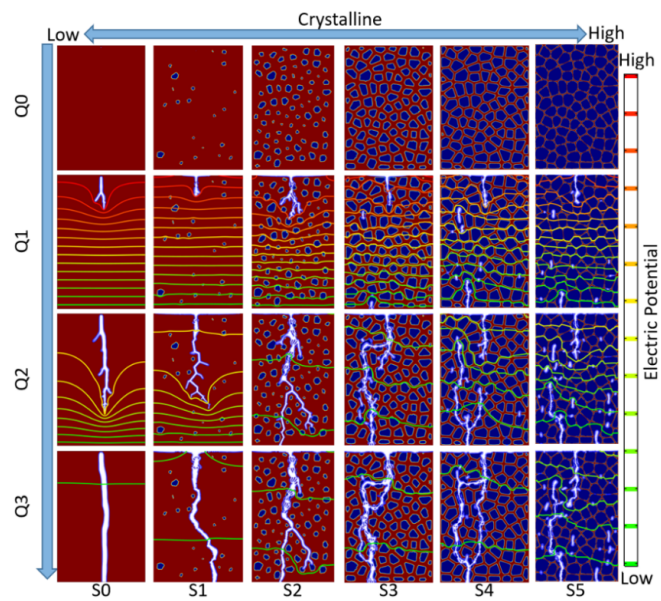

Fig. 3. Electrical treeing of different state in evolution process with S0–S5.

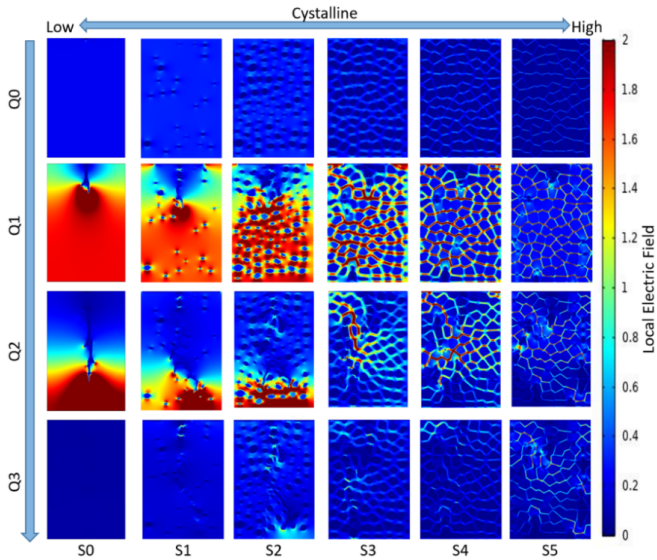

Fig. 4. Electric field distribution of different states in evolution process with S0–S5.

position when breakdown begin with a local defect-induced breakdown. This phenomenon is more obvious with the increase of crystallinity.

From the perspective of transverse, the model starts the process of breakdown at Q1. In the process of breakdown, the equipotential lines at the tip of the electrical treeing are dense and the potential is large. It is consistent with the characteristic that the maximum electric field is reached near Q1 in Fig. 2(a). The electric field gradually decreases once the breakdown occurs.

Figure 4 shows the distribution of electric field in dielectric breakdown from S0 to S6. The strong electric field is mainly concentrated in the grain boundary, especially at the tip of the electrical treeing. The dielectric breakdown forms the damage field causing the electric field on its path to be weak.

In Fig. 5(a), the curves represent the dielectric permittivity change during the breakdown evolution with S0–S5. As shown in Fig. 5(a), before reaching the breakdown condition, the dielectric permittivity decreases relatively slighter with the increase in charge density, while it fluctuates greatly

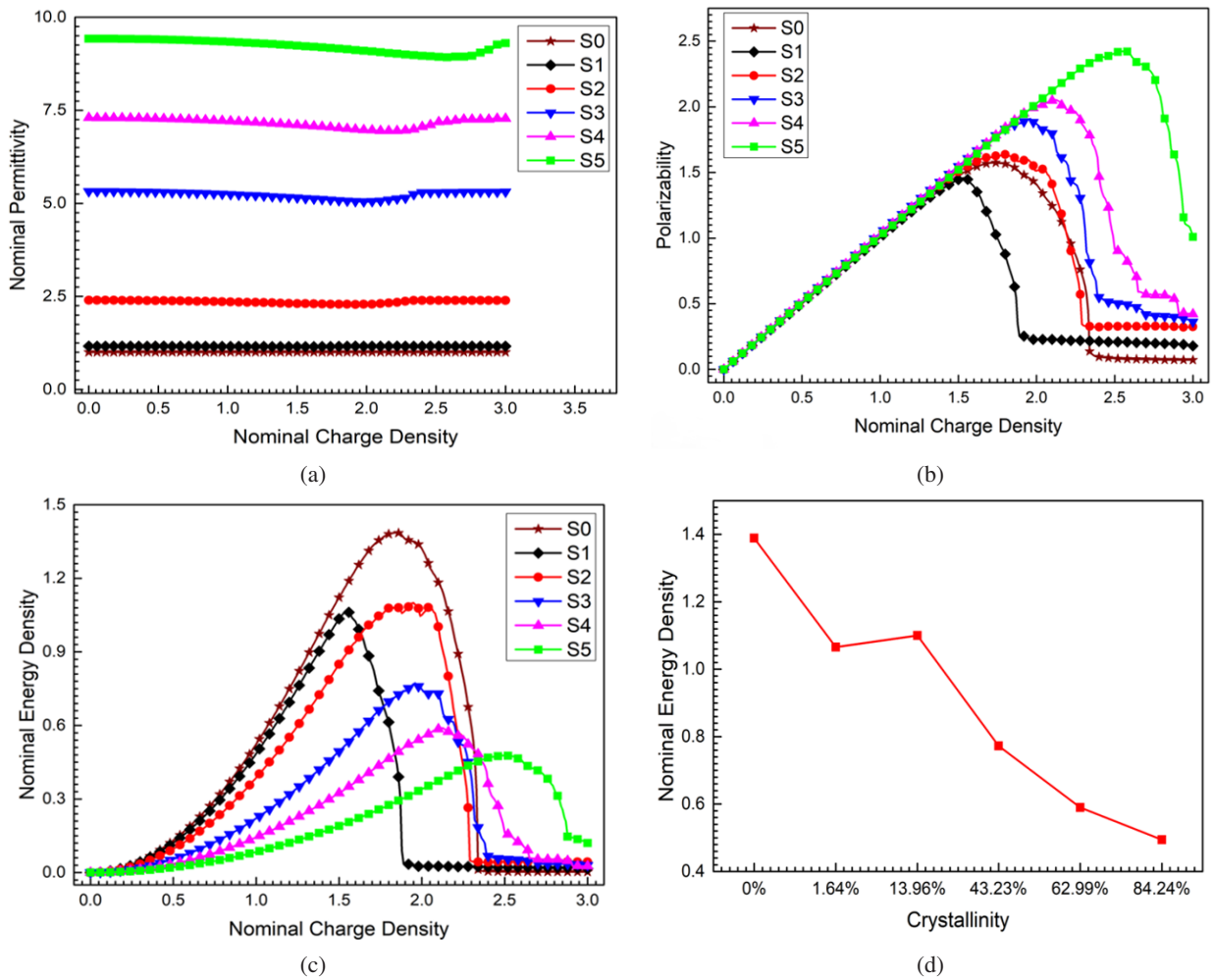

Fig. 5. (a) The change of nominal dielectric permittivity with nominal charge in S0–S5; (b) The change of polarizability with nominal charge in S0–S5; (c) The change of nominal energy density with charge in S0–S5 and (d) The relationship between energy storage density and crystallinity.

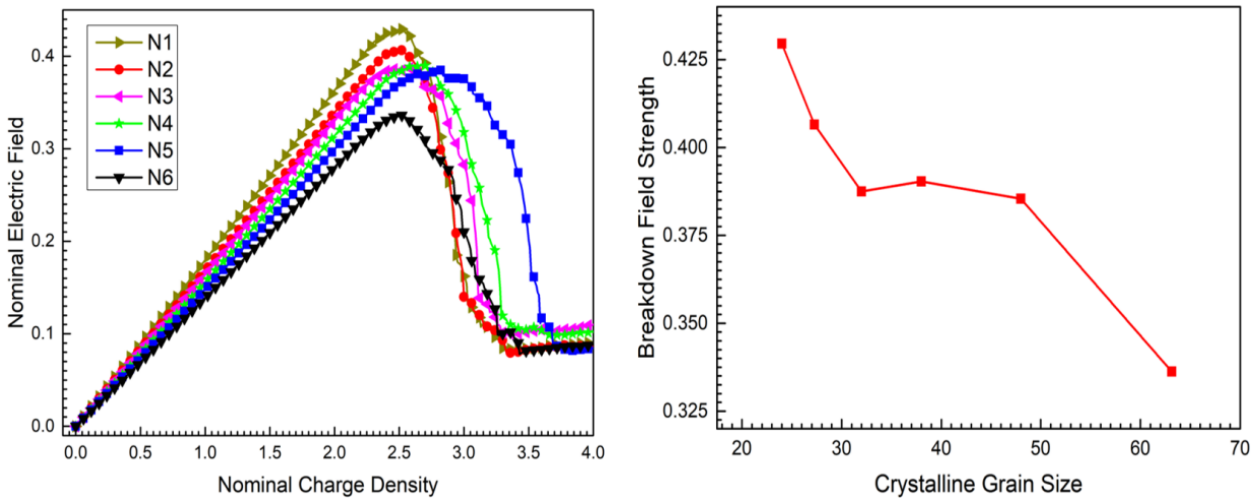

(a) (b)

Fig. 6. (a) Field-charge-density relation in N1–N6 and (b) The relationship between grain size and breakdown field strength in N1–N6.

at the beginning of breakdown. From S0 to S5, the dielectric permittivity increases with the increase in crystallinity. Combined with Fig. 2(c), the breakdown field strength decreases with the increase in dielectric permittivity. In Fig. 5(b), the polarizability is similar to the change in the electric field. The polarizability increases with the increase of charge density linearly, and starts to decline after reaching the breakdown condition. The linear part of the curve from S0 to S5 almost coincides. The maximum polarizability of phase-field model increases with the increase of crystallinity. Figure 5(d) shows the relationship between the crystallinity of the phase-field model and energy storage density, in which the abscissa represents the crystallinity with S0–S5. According to Figs. 5(c) and 5(d), with the increase in crystallinity, the energy storage density decreases as a whole.

In summary, with increasing crystallinity, the breakdown path will change from centralized and single to decentralized and complex, and the breakdown field strength will decrease. When the crystallinity is higher than 43.23%, the phase-field model is biased to induce global breakdown from local defects achieving lower breakdown field strength. Corresponding to it, the energy storage density achieved by the model also tends to decrease with the increase in crystallinity. In the first stage of phase transition, the size of the grain boundary is relatively large, and the electrostatic potential energy in the phase-field model is mainly calculated by the grain boundary part of formula (5). With the increasing crystallinity, the dielectric permittivity increases and the breakdown field strength decreases. Compared with the dielectric permittivity, the breakdown field strength has a greater effect on the energy storage density. In the pure phase, the breakdown field strength and the energy storage density are the highest. When the crystal phase appears, the breakdown field strength decreases and the energy storage density decreases. With the transition of crystalline phase, the energy storage density first increases to the maximum in impure phase and then decreases. The maximum value is obtained at the crystallinity of 13.96% in the process of phase transition. It indicates that the change of the ferroelectric ceramics microstructure can optimize the energy storage density in the process of crystallinity growth.

3.2. *The Second Stage from N1 to N6*

Figure 6(a) shows the relationship between electric field and nominal charge density with N1–N6. Figure 6(b) shows the breakdown field strength and average grain size of the corresponding models. A downward trend of breakdown field

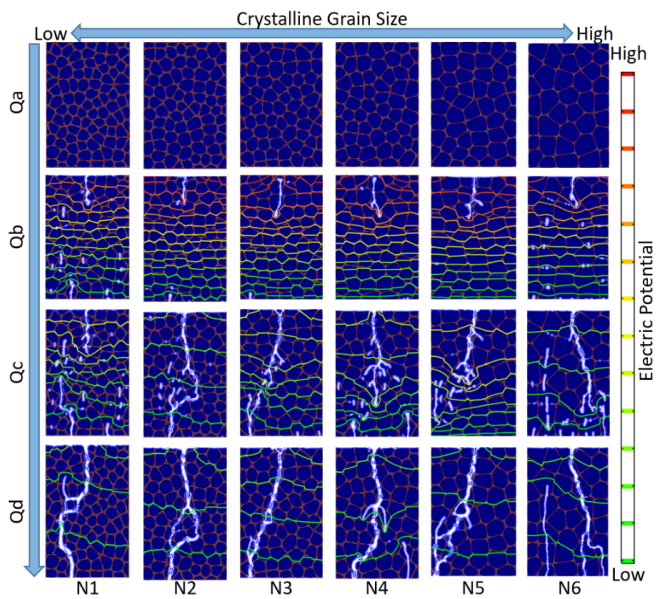

Fig. 7. Electrical treeing of different state in evolution process with N1–N6.

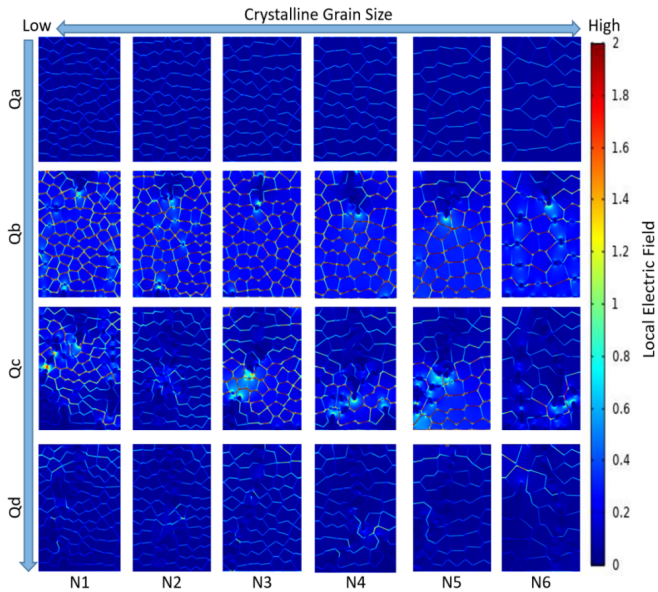

Fig. 8. Electric field distribution of different states in evolution process with N1–N6.

Table 2. The corresponding nominal charge density in evolution process with N1–N6.

Charge density	N1	N2	N3	N4	N5	N6
Qa	0.48	0.53	0.56	0.59	0.60	0.62
Qb	2.75	2.60	2.55	2.70	2.90	2.73
Qc	2.90	3.15	3.10	3.20	3.45	3.25
Qd	4.0	4.0	4.0	4.0	4.0	4.0

strength is shown in Fig. 6 with increasing average size. The change of breakdown field strength from N3 to N5 is not obvious.

Figures 7 and 8 show the evolution of electrical treeing and electric field distribution of the samples from N1 to N6, respectively. The Qa–Qd in Figs. 7 and 8 is the charge density imposed in both ends of the samples. The specific corresponding charge density is shown with Qa–Qd in Table 2. In Fig. 7, the samples with increasing average grain size are shown from left to right. In order to compare with each other, each different sample maintains the same grain boundary

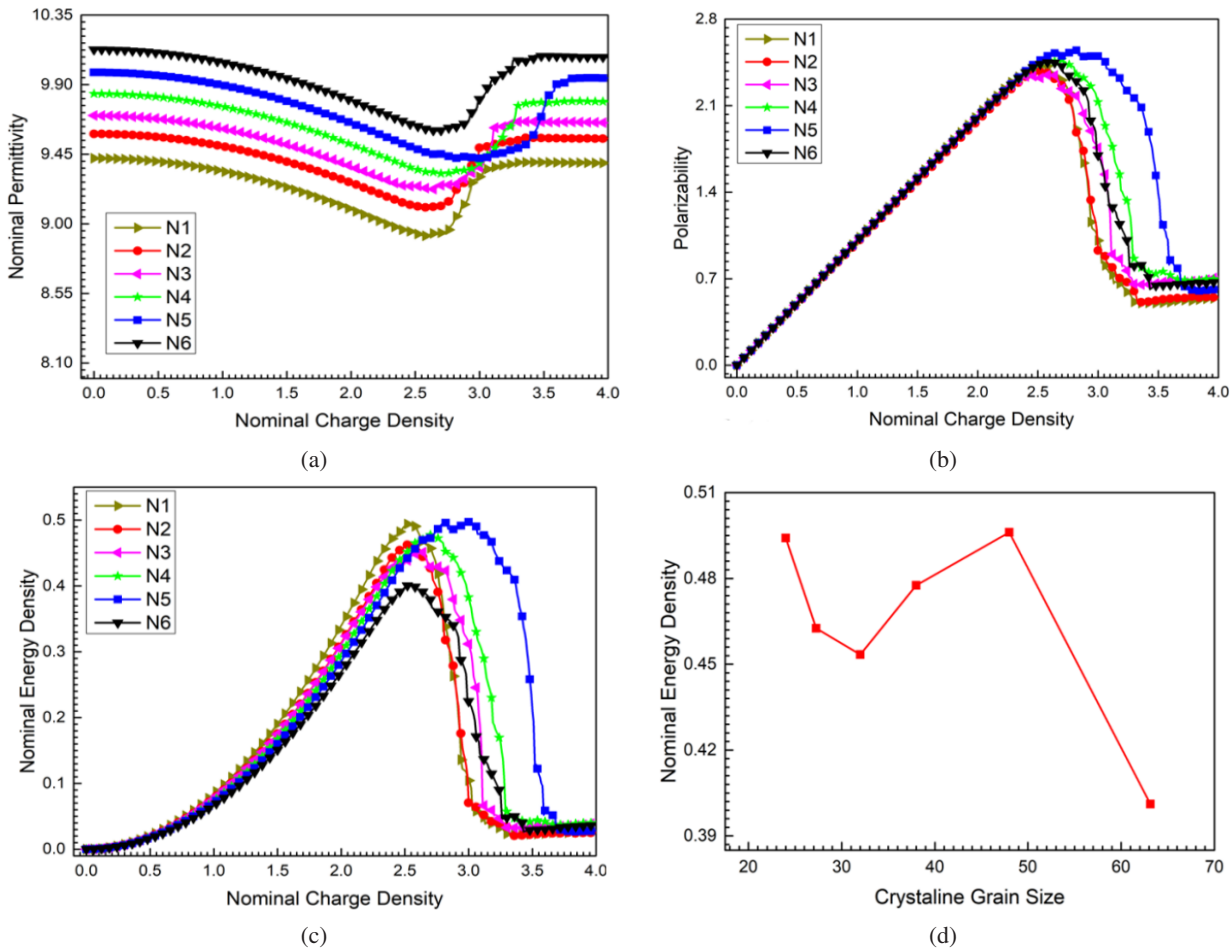

Fig. 9. (a) The change of nominal dielectric permittivity with nominal charge in N1–N6; (b) The change of polarizability with nominal charge in N1–N6; (c) The change of nominal energy density with charge in N1–N6; (d) The relationship between the energy storage density and average grain size.

size. The white path (Fig. 7) is the distribution of the electrical treeing and the curves of different colors are equipotential lines. As shown in Fig. 7, the distribution of the electrical treeing is complex, distributed in the multiple places of samples. At the beginning of the breakdown, the electric field intensity is the highest and the equipotential lines are dense concentrating at the tip of the electrical treeing. After breakdown behavior is completed, the electric field strength slips to a low value. Figure 8 shows the electric field distribution during the evolution for dielectric breakdown, and the legend on the right side shows the corresponding value of electric field.

Figure 9(a) shows the change of dielectric permittivity during the dielectric breakdown with N1–N6. The change of dielectric permittivity in Fig. 9(a) is similar to Fig. 5(a). Before the breakdown appears, the dielectric permittivity decreases with the increase of charge density. In the charge-free state, the dielectric permittivity increases with the average grain size increasing. Figure 9(b) shows the change of polarizability during the dielectric breakdown with N1–N6. The changing trend of the polarizability of each size is almost the same, and the linear part of the curve from N1 to N6 almost coincides. N5 and N1 can achieve maximum and minimum polarizability, respectively. As shown in Fig. 9(c), N5 can achieve the highest energy storage density and N6 can achieve the lowest energy storage density. The energy storage density with N1–N6 is drawn into a polyline in Fig. 9(d), in which the abscissa represents the average grain size. According to Fig. 9(d), with the average grain size increasing, the energy storage density first decreases, then increases, finally decreases, and reaches the highest at N5. The main reason for this is that the breakdown field strength has no significant change from N3 to N5. Thus, at this point, the main factor determining the energy storage density is the continuously increasing dielectric permittivity, which results in the storage energy density increasing from N3 to N5.

In conclusion, when the grain size increases, the dielectric permittivity increases, but the overall breakdown field strength shows a downtrend. In the process of the grain growth in the second stage of the phase transition, the energy storage density of the ferroelectric ceramics first decreases, then increases and finally decreases. In the second stage of the phase transition with a high crystallinity, it is common for inducing breakdown by local defect. There is an exact value of average grain size to optimize the storage energy. N5 can achieve the maximum storage energy density as the average grain size is 50. The corresponding volume fraction of N5 is 2.08%.

4. Conclusion

We proposed a method to simulate the process of phase transition. The method couple phase-field for dielectric breakdown model with the microstructures during the phase transition to explore the correlative mechanism of microstructure on energy storage characteristics. After simulating the phase transition process of amorphous/nanocrystalline and polycrystalline, the results show that multiphase ceramics have an optimal energy storage in the process of amorphous polycrystalline transformation, where the energy storage density reaches the maximum when the crystallinity is 13.96% and the volume fraction of grain is 2.08%.

Acknowledgments

This work was supported by the youth project of Guangdong Foshan joint fund of Guangdong Natural Science Foundation (Grant No. 2020A1515110601 and Grant No. 2019A1515110444), the National Natural Science Foundation of China (No: 61804029), and the Project of Foshan Science and Technology Innovation Team (No: FS0AA-KJ919-4402-0062).

References

[1]W. Feng, V. S. Avvaru, R. R. Maca, S. J. Hinder, M. C. Rodriguez and V. Etacheri, Realization of high energy density sodium-ion hybrid capacitors through interface engineering of pseudocapacitive 3D-CoO-NrGO hybrid anodes, *ACS Appl. Mater Interfaces*. **13**, 27999 (2021).

[2]X. Hao, A review on the dielectric materials for high energy-storage application, *J. Adv. Dielec*. **03**, 01 (2013).

[3]L. Hou, C. Li, X. Wang, X. Wang, T. Wang and Y. Huan, Superior energy storage efficiency through tailoring relaxor behavior and band energy gap in KNN-based ferroelectric ceramic capacitors, *J. Adv. Dielect*. **12**, 2242001 (2022).

[4]F. Li, X. Hou, J. Wang, H. Zeng, B. Shen and J. Zhai, Structure-design strategy of 0–3 type (Bi0.32Sr0.42Na0.20)TiO3/MgO composite to boost energy storage density, efficiency and charge-discharge performance, *J. Eur. Ceram. Soc*. **39**, 2889 (2019).

[5]H. Liang, Y. Zhang, S. Hao, L. Cao, Y. Li, Q. Li, D. Chen, X. Wang, X. Guo and H. Li, Fast potassium storage in porous CoV2O6 nanosphere@graphene oxide towards high-performance potassium-ion capacitors, *Energy Stor. Mater*. **40**, 250 (2021).

[6]C. Sun, X. Zhang, C. Li, K. Wang, X. Sun, F. Liu, Z.-S. Wu and Y. Ma, A safe, low-cost and high-efficiency presodiation strategy for pouch-type sodium-ion capacitors with high energy density, *J. Energy Chem*. **64**, 442 (2022).

[7]J.-Y. Tan, J.-T. Su, Y.-J. Wu, C.-L. Huang, P.-Y. Cheng, Y.-A. Chen and S.-Y. Lu, Hollow porous α-Fe2O3 nanoparticles as anode materials for high-performance lithium-ion capacitors, *ACS Sustain. Chem. Eng*. **9**, 1180 (2021).

[8]J. Wang, X. Nie, Z. Peng, X. Lei, P. Liang, Z. Yang and X. Chao, Ultra-fast charge-discharge and high energy storage density realized in NaNbO3–La(Mn0.5Ni0.5)O3 ceramics, *Ceram. Int*. **47**, 28493 (2021).

[9]J. Zheng, G. Xing, L. Zhang, Y. Lu, L. Jin and J. P. Zheng, A mini-review on highperformance anodes for lithiumion capacitors, *Batter. Supercaps*. **4**, 897 (2021).

[10]Y. I. Kim, E. Samuel, B. Joshi, M.-W. Kim, T. G. Kim, M. T. Swihart and S. S. Yoon, Highly efficient electrodes for supercapacitors using silver-plated carbon nanofibers with enhanced mechanical flexibility and long-term stability, *Chem. Eng. J*. **353**, 189 (2018).

[11]D. Zhang, J. Wang, Q. Wang, S. Huang, H. Feng and H. Luo, Nitrogen self-doped porous carbon material derived from metal-organic framework for high-performance super-capacitors, *J. Energy Storage* **25**, 100904 (2019).

[12]S. Zheng, X. Li, B. Yan, Q. Hu, Y. Xu, X. Xiao, H. Xue and H. Pang, Transition-metal (Fe, Co, Ni) based metal-organic frameworks for electrochemical energy storage, *Adv. Energy Mater*. **7**, 1602733 (2017).
[13]B. Luo, X. Wang, Y. Wang and L. Li, Fabrication, characterization, properties and theoretical analysis of ceramic/PVDF composite flexible films with high dielectric constant and low dielectric loss, *J. Mater. Chem. A* **2**, 510 (2014).
[14]Z. Pan, S. Xing, H. Jiang, J. Liu, S. Huang and J. Zhai, Highly enhanced discharged energy density of polymer nanocomposites via a novel hybrid structure as fillers, *J. Mater. Chem. A* **7**, 15347 (2019).
[15]H. Wang, J. Liu, J. Zhai, B. Shen and M. Cain, Ultra high energy-storage density in the barium potassium niobate-based glass-ceramics for energy-storage applications, *J. Am. Ceram. Soc*. **99**, 2909 (2016).
[16]N. Luo, K. Han, F. Zhuo, C. Xu, G. Zhang, L. Liu, X. Chen, C. Hu, H. Zhou and Y. Wei, Aliovalent A-site engineered AgNbO3 lead-free antiferroelectric ceramics toward superior energy storage density, *J. Mater. Chem. A* **7**, 14118 (2019).
[17]N. Luo, K. Han, L. Liu, B. Peng, X. Wang, C. Hu, H. Zhou, Q. Feng, X. Chen and Y. Wei, Lead-free Ag1-3*x*La*x*NbO3 antiferroelectric ceramics with high energy storage density and efficiency, *J. Am. Ceram. Soc*. **102**, 6 (2019).
[18]P.-F. Li, W.-Q. Liao, Y.-Y. Tang, H.-Y. Ye, Y. Zhang and R.-G. Xiong., Unprecedented ferroelectric-antiferroelectric-paraelectric phase transitions discovered in an organic-inorganic hybrid perovskite, *J. Am. Ceram. Soc*. **139**, 8752 (2017).
[19]R. Xu, J. Tian, Q. Zhu, T. Zhao, Y. Feng, X. Wei and Z. Xu, Effects of La-induced phase transition on energy storage and discharge properties of PLZST ferroelectric/antiferroelectric ceramics, *Ceram. Int*. **43**, 13918 (2017).
[20]T. Zhang, W. Li, Y. Hou, Y. Yu, R. Song, W. Cao and W. Fei, High-energy storage density and excellent temperature stability in antiferroelectric/ferroelectric bilayer thin films, *J. Am. Ceram. Soc*. **100**, 3080 (2017).
[21]K. P. Andryushin, A. V. Nagaenko, S. V. Khasbulatov, L. A. Shilkina, E. V. Glazunova, S. I. Dudkina, I. N. Andryushina and L. A. Reznichenko, Microstructure features of the BST/(Mg, Ln)-ceramic, *J. Adv. Dielectr*. **12**, 2160005 (2022).
[22]Z. Cai, X. Wang, B. Luo, W. Hong, L. Wu and L. Li, Multiscale design of high-voltage multilayer energy-storage ceramic capacitors, *J. Am. Ceram. Soc*. **101**, 1607 (2018).
[23]H. Pan, A. Kursumovic, Y. H. Lin, C. W. Nan and J. L. MacManus-Driscoll, Dielectric films for high performance capacitive energy storage: Multiscale engineering, *Nanoscale* **12**, 19582 (2020).
[24]N. A. Shvetsova, I. A. Shvetsov, M. A. Lugovaya, E. I. Petrova and A. N. Rybyanets, Microstructure characterization and properties of porous piezoceramics, *J. Adv. Dielectr*. **12**, 2160006 (2022).
[25]Y. Y. Cheng, L. Liu, Y. Huang, L. Shu, Y. X. Liu, L. Wei and J. F. Li, All-inorganic flexible (K, Na)NbO3-based lead-free piezoelectric thin films spin-coated on metallic foils, *ACS Appl. Mater. Interfaces*. **13**, 39633 (2021).
[26]M. Rahimabady, L. Lu and K. Yao, Nanocomposite multilayer capacitors comprising BaTiO3@TiO2 and poly(vinylidene fluoride-hexafluoropropylene) for dielectric-based energy storage, *J. Adv. Dielectr*. **04**, 1450009 (2014).
[27]B. Yang, C. Li, M. Liu, R. Wei, X. Tang, L. Hu, W. Song, X. Zhu and Y. Sun, Design of flexible inorganic BiFe0.93Mn0.07O3 ferroelectric thin films for nonvolatile memory, *J. Materiom*. **6**, 600 (2020).
[28]H. Yu, C. C. Chung, N. Shewmon, S. Ho, J. H. Carpenter, R. Larrabee, T. Sun, J. L. Jones, H. Ade, B. T. O'Connor and F. So, Flexible inorganic ferroelectric thin films for nonvolatile memory devices, *Adv. Funct. Mater*. **27**, 1700461 (2017).
[29]H. Bartzsch, D. Glöß, B. Böcher, P. Frach and K. Goedicke, Properties of SiO_2 and Al_2O_3 films for electrical insulation applications deposited by reactive pulse magnetron sputtering, *Surf. Coat. Technol*. **174–175**, 774 (2003).
[30]F. C. Carreri, R. Bandorf, H. Gerdes, M. Vergöhl and G. Bräuer, Highly insulating alumina films by a bipolar reactive MF sputtering process with special arc handling, *Surf. Coat. Technol*. **290**, 82 (2016).
[31]B. V. T. Hanby, B. W. Stuart, M. Gimeno-Fabra, J. Moffat, C. Gerada and D. M. Grant, Layered Al2O3-SiO2 and Al2O3-Ta2O5 thin-film composites for high dielectric strength, deposited by pulsed direct current and radio frequency magnetron sputtering, *Appl. Surf. Sci*. **492**, 328 (2019).
[32]B. Ma, M. Narayanan and U. Balachandran, Dielectric strength and reliability of ferroelectric PLZT films deposited on nickel substrates, *Mater. Lett*. **63**, 1353 (2009).
[33]C. Chen, H. Hao, T. Wang, J. Cheng, Z. Luo, L. Zhang, M. Cao, Z. Yao and H. Liu, Nano-BaTiO3 phase transition behavior in coated BaTiO3-based dielectric ceramics, *Ceram. Int*. **45**, 7166 (2019).
[34]T. B. Wermuth, J. Venturini, W. C. Guaglianoni, A. M. Tonelli, E. A. Chavarriaga, S. Arcaro, M. N. Baibich and C. P. Bergmann, Enhancement of magnetic and dielectric properties of KNbO3–CoFe2O4 multiferroic composites via thermal treatment, *Ceram. Int*. **47**, 4874 (2021).
[35]L. Zhao, J. C. Su and C. L. Liu, Review of developments on polymers' breakdown characteristics and mechanisms on a nanosecond time scale, *AIP Adv*. **10**, 035206 (2020).
[36]L. Yang, X. Kong, F. Li, H. Hao, Z. Cheng, H. Liu, J.-F. Li and S. Zhang, Perovskite lead-free dielectrics for energy storage applications, *Prog. Mater. Sci*. **102**, 72 (2019).
[37]L. Zhao, A formula to calculate solid dielectric breakdown strength based on a model of electron impact ionization and multiplication, *AIP Adv*. **10**, 025003 (2020).
[38]L. Zhao, Theoretical calculation on formative time lag in polymer breakdown on a nanosecond time scale, *IEEE Trans. Dielectr. Electr. Insul*. **27**, 1051 (2020).
[39]Z. Cai, X. Wang and L. Li, Phase-field modeling of electromechanical breakdown in multilayer ceramic capacitors, *Adv. Theory Simul*. **2**, 1800179 (2018).
[40]Z. Cai, X. Wang, L. Li and W. Hong, Electrical treeing: A phase-field model, *Extreme Mech. Lett*. **28**, 87 (2019).
[41]Z. Mi, Y. Zhang, X. Hou and J. Wang, Phase field modeling of dielectric breakdown of ferroelectric polymers subjected to mechanical and electrical loadings, *Int. J. Solids Struct*. **217–218**, 123 (2021).
[42]K. Chaitanya Pitike and W. Hong, Phase-field model for dielectric breakdown in solids, *J. Appl. Phys*. **115**, 044101 (2014).
[43]W. Hong and K. C. Pitike, *Procedia IUTAM* **12**, 73 (2015).
[44]Z. Cai, X. Wang, B. Luo, W. Hong, L. Wu and L. Li, Dielectric response and breakdown behavior of polymer-ceramic nanocomposites: The effect of nanoparticle distribution, *Compos. Sci. Technol*. **145**, 105 (2017).
[45]H. Ye, F. Yang, Z. Pan, D. Hu, X. Lv, H. Chen, F. Wang, J. Wang, P. Li, J. Chen, J. Liu and J. Zhai, Significantly improvement of comprehensive energy storage performances with lead-free relaxor ferroelectric ceramics for high-temperature capacitors applications, *Acta Mater*. **203**, 16484 (2021).
[46]Z. Cai, X. Wang, W. Hong, B. Luo, Q. Zhao and L. Li, Grain-size-dependent dielectric properties in nanograin ferroelectrics, *J. Am. Ceram. Soc*. **101**, 5487 (2018).
[47]K. M. Johnson, Variation of dielectric constant with voltage in ferroelectrics and its application to parametric devices, *J. Appl. Phys*. **33**, 2826 (1962).